

## RESEARCH ARTICLE

10.1029/2018JA025773

## Key Points:

- Influence of SGR X-ray bursts on Earth's ionosphere and middle atmospheric plasma properties is examined
- Extensive modeling of VLF signal modulation due to a complex SGR X-ray burst is performed
- GEANT4 Monte Carlo simulation and ion chemistry model are employed in numerical reconstruction of observed signal modulation

## Correspondence to:

S. Palit,  
souravspace@gmail.com

## Citation:

Palit, S., Raulin, J.-P., & Correia, E. (2018). Lower ionospheric plasma-chemical evolution and VLF signal modulation by a series of SGR X-ray bursts: Numerical simulation with an ion-chemistry model. *Journal of Geophysical Research: Space Physics*, 123, 7930–7942. <https://doi.org/10.1029/2018JA025773>

Received 10 JUN 2018

Accepted 6 SEP 2018

Accepted article online 8 SEP 2018

Published online 24 SEP 2018

## Lower Ionospheric Plasma-Chemical Evolution and VLF Signal Modulation by a Series of SGR X-Ray Bursts: Numerical Simulation With an Ion-Chemistry Model

Sourav Palit<sup>1</sup> , Jean-Pierre Raulin<sup>1</sup>, and Emilia Correia<sup>1,2</sup>

<sup>1</sup>Centro de Radio Astronomia e Astrofísica Mackenzie, Universidade Presbiteriana Mackenzie, São Paulo, Brazil, <sup>2</sup>Instituto Nacional de Pesquisas Espaciais, São José dos Campos, Brazil

**Abstract** The X-ray and gamma ray radiation from astrophysical transient sources, like X-ray bursts from soft gamma repeaters (SGRs) and gamma ray bursts (GRBs), can affect the plasma properties of the lower ionosphere and middle atmosphere. Multiple very low frequency (VLF) receivers in South America, with an unprecedented high time resolution of 20 ms, detected one such series of bursts from SGR J1550-5418 on 22 January 2009. Due to lack of other suitable means of observation corresponding to the lower part of Earth's ionosphere (~60–100 km), the VLF detection and analysis of transient ionizing events (mostly of solar origin) has emerged as an excellent method to investigate various chemical and plasma characteristics at these heights. Extragalactic events, like SGR bursts and GRBs, with sharp modulation in their radiation time profile and very high energy photon abundances provide most unique opportunities of such studies with the possibility of extending even lower heights in the atmosphere. Here, for the first time, an extensive computer model, consisting of the combination of Monte Carlo ionization rate computation, a one dimensional atmospheric chemistry module, and VLF waveguide mode calculation, for the reconstruction of VLF signal modulation produced by SGR X-ray burst starting from the observed spectrum and lightcurve of the event is presented. We gain some valuable insight on the nature of chemical and dynamic evolution over the entire height range of the atmosphere examined from the exercise.

### 1. Introduction

Response of Earth's atmosphere to celestial ionizing events has emerged as a very important area of research in last few decades. They have been proved to be valuable in both investigating the atmospheric chemical and dynamical characteristics (Fishman & Inan, 1988; Inan et al., 2007; Mendillo et al., 1974; Mitra, 1968; Palit et al., 2015; Qian et al., 2012; Raulin et al., 2013; Usoskin et al., 2009) and tracking and analyzing the source and characteristics of those events (Grubor et al., 2008; Nina & Čadež, 2014; Palit et al., 2016; Tanaka et al., 2008; Žigman et al., 2007). The ionized part of the atmosphere, namely, the ionosphere, has particularly been at the center of interest. Along with many terrestrial influences, the Sun is the predominant extraterrestrial driver of various dynamic evolution at this part of the atmosphere. Apart from the fact that the ionosphere itself is the result of the ionizing interaction mainly of solar ultraviolet radiation (Nicolet & Aikin, 1960; Watanabe, 1958; Watanabe et al., 1955), the effect of X-rays from solar flares and energetic particles from various solar eruptive events, like flares and coronal mass ejection (CME), has been studied extensively (Kolarski & Grubor, 2014; Liu et al., 1996; Mariska & Oran, 1981; McRae & Thomson, 2004; Palit et al., 2013, 2015; Thomson & Clilverd, 2001; Velinov et al., 2013).

For the lower ionosphere, remote sensing using very low frequency (VLF) radio waves is an excellent tool to investigate the dynamic changes in plasma environment during such events. Due to large air drag at these heights, the satellite measurements are unlikely, and scientific balloons cannot reach those heights. Radio signals at higher frequencies, like those used in ionosondes and incoherent scatter radars, are usually of very small and insignificant echoes (due to very small electron density,  $\sim 10^3 \text{ cm}^{-3}$  at those heights; Hargreaves, 1992; Mathews et al., 1982) and prone to be masked by interference and noise. The ionizing interaction of photons and charged particles with neutrals, followed by the chemical stabilization processes, modifies the ambient electron (ion) density in ionosphere, which is designated primarily by Wait's formula (Wait & Spies, 1964). The immediate manifestation of such evolution on the absorption level of the electromagnetic



**Figure 1.** The figure shows the NPM-EACF and NPM-ROI VLF propagation paths on 22 January 2009 at 05:18 UT in white lines. The projections of the subflare point and of the Sun on the Earth's surface are represented by the black and the yellow circles, respectively. The dark and light blue areas indicate, respectively, the regions under nighttime conditions and under solar illumination. At the south of the thick black line, the regions of the Earth illuminated by the flaring object is located. The figure is taken from Raulin et al. (2014). NPM = Lualualei, Hawaii; EACF = Estação Antarctica Commandante Ferraz; ROI = Radio Observatorio do Itapetinga.

energy associated with the VLF radio signal, propagated between a pair of transmitter and receiver, causes modification in the amplitude and phase of the received signal.

The energetic photons (X-ray and  $\gamma$ -ray) reaching the Earth's atmosphere from extrasolar transient events like gamma ray bursts (GRB) and soft gamma repeater (SGR) penetrate deep (as low as  $\sim 20$  km; Inan et al., 2007) into the atmosphere and ionize the neutrals, causing temporary modification in ion densities, hence affecting the VLF propagation. Though very few of such events have been detected with VLF so far (Fishman & Inan, 1988; Hurley et al., 1999; Mondal et al., 2012; Nina et al., 2015; Tanaka et al., 2007), they are of utmost importance requiring thorough investigation (see Raulin et al., 2014, for some discussions). First, any individual burst from such a source, being very short in duration (with respect to the chemical recombination time scales at lower ionospheric heights), produces an ionizing disturbance, resembling a spike (or effectively a delta function in time). Each of these spikes may provide us an excellent opportunity to investigate the chemical evolution following the disturbance, to accurately determine the electron (ion) recombination rates at these heights. The second aspect is regarding the detection and probable characterization of the cosmic transient sources; as in many of such events, the conventional mode of detection, like space-based high energy X-ray and  $\gamma$ -ray detectors, gets inactive due to Earth's occultation or saturation, in which cases VLF detection and analysis may be a viable option.

The observation (Raulin et al., 2014) of VLF signal modulation following such spikes of ionization used here is due to a series of X-ray bursts from a SGR. Many of such bursts from SGR J1550-5418 on 22 January 2009 were detected by VLF receivers in two propagation paths (shown in Figure 1) between transmitter NPM (Lualualei, Hawaii, 21.4 N, 158.15 W, frequency: 21.4 kHz) and the receivers Estação Antarctica Commandante Ferraz (EACF, 62.72 S, 58.42 W) and Radio Observatorio do Itapetinga (ROI, 23.18 S, 46.55 W), which are part of the Atmospheric Weather Electromagnetic System for Observation Modeling and Education array (Cohen et al., 2009). Uninterrupted monitoring of several bursts of SGR J1550-5418 on 22 January 2009 along those two paths was performed. Depending on whether the VLF signal modulations due to consecutive bursts are distinct or coupled (i.e., a signal modulation corresponding to a certain peak in the X-ray burst does not occur during the recovery of the previous one or not), the events are classified as simple and complex types. Nevertheless, all of the modulations have the common feature of sudden decrease in VLF amplitude followed by a gradual recovery, the later signifying the recovery of the ionospheric characteristics by electron, ion-neutral recombination processes. The aim of this paper is to reconstruct these VLF modulation with a framework of three step modeling process. This consists first the calculation of ionization due to the X-ray/ $\gamma$ -ray in the lower ionosphere and middle atmospheric heights using a Monte Carlo simulation, subsequent modeling of the recovery by chemical recombination processes with an ion-chemistry evolution model and finally the estimation of VLF signal modulation with waveguide mode calculations.

According to the mode theory of VLF radio wave propagation (Budden, 1961; Galejs, 1972; Wait, 1962), the signal at any receiving location is the resultant of the various modes propagating in the waveguide consisting of the surface of the Earth and the lower boundary of the ionosphere, where the waves suffer multiple reflections during propagation. The VLF phase and amplitude are sensitive to various parameters along the path, such as lower ionospheric electrical conductivity, presence of atmospheric currents and magnetic fields, ground conductivity and hence presence of solid crust or ocean, propagation distance between a pair of transmitter and receiver, and so forth. The multiparametric nature of the process makes the analysis or prediction of VLF signal at any given atmospheric condition complicated. Interpretation or modeling of VLF signal has been performed mainly with computation model of waveguide mode theory. For this purpose, mode search algorithms, such as those employed in Long Wave Propagation Capability code (LWPC; J. A. Ferguson, 1998), have been used extensively.

The most common approach of analysis of VLF signal modulation by transient ionizing events has been to estimate the changes in ionospheric parameters, like electron and ion densities and conductivity revealed by those VLF observations (see Schmitter, 2013; Thomson et al., 2005, e.g.). The efforts of interpreting or modeling the observed VLF signal modulation by calculating the influence of source radiation on the ionospheric or atmospheric parameters and then estimating the corresponding changes in propagation characteristic are handful. Along the line of the later approach, Palit et al. (2013) presented one such model calculations for the observed amplitude modulation during a X and a M class solar flare. Palit et al. (2015) also formulated and quantified the observed delay between peaks of the flare X-ray and the corresponding sudden ionospheric disturbances (SIDs), in terms of the flare parameters (like intensity and sharpness of the incident X-ray lightcurve) and atmospheric reaction rate coefficients. The modeling was also extended to investigate the possibility of extracting the information on the low-energy X-ray flare spectrum from VLF observation (Palit et al., 2016). These studies are important steps forward in both of the aspects stated earlier, that is, characterization of atmospheric chemistry/dynamics and that of radiation source properties. For events other than solar flares, the examples are even fewer. Inan et al. (2007) presented their simulation on the VLF signature of a SGR from a magnetar, based on calculation of ionization by a model spectrum, electron density evolution, and application of LWPC. Tanaka et al. (2008) tried, instead, Finite Difference Time Domain (FDTD) method, suitable for short propagation path to model the ionospheric effects of a giant  $\gamma$ -ray flare. As described in the subsequent sections of this paper, our method of reconstruction of VLF signal amplitude during SGR X-ray bursts follows the second approach and is analogous to that presented in Palit et al. (2013). In this work, for the first time, such an extensive computer simulation of the influence of extraterrestrial ionizing events on the Earth's atmosphere and VLF wave propagation is performed and reported. It starts with the observed spectrum and lightcurve of the SGR X-ray burst event and tries to follow the true physics and chemistry evolution of the atmospheric region of influence. We also try to improve our insight on the nature and dynamics of the ion-chemical processes evolving in disturbed part of the atmosphere.

In section 2, we describe briefly the observations to be interpreted or reconstructed with our computational model. For the details of the VLF data acquisition and analysis, we refer readers to Raulin et al. (2014). In section 3, we elaborate some physical processes competing in the evolution and detection of the ionizing response in VLF. This discussion will be helpful to grasp the model steps and comparison of model results with observation, presented in the following two sections. This is also quite important in understanding the modifications in the model, made over its earlier version employed to study the response of VLF wave propagation to solar flares (Palit et al., 2013). First, section 3 contains a brief qualitative account of the propagation characteristics of VLF radio waves and the basics of how the ionizing radiation from those bursts cause the modification in the plasma characteristics of lower ionosphere and middle atmosphere which affects the VLF signal. Second, we dig a little deeper into the typical spectral and timing characteristics of the above-mentioned extragalactic sources, namely, the SGR X-ray bursts, and how should they differ in producing the ionospheric or rather atmospheric response than those by solar flares. Section 4 contains the description of the model, consisting the outline of the computation method for Monte Carlo ionization process accompanied by the choice of input spectrum and light-curve and basics of ion chemistry model and LWPC for the simulation of atmospheric and VLF response. In section 5, we demonstrate the model results, emphasizing on the simulated VLF amplitude modulation and how do those commensurate with the actual observation. In the last section, we make some discussions and concluding remarks.

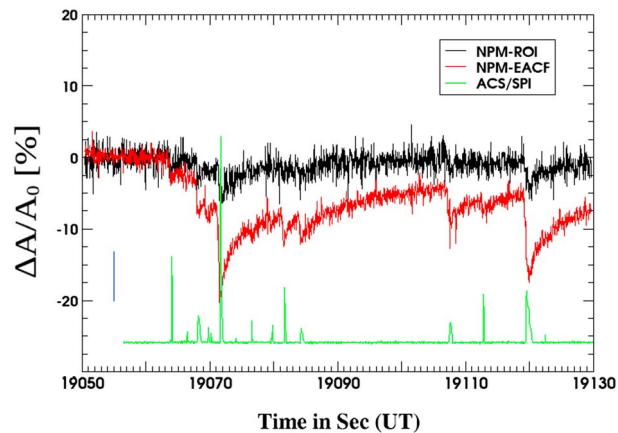


**Figure 2.** Modulation in very low frequency amplitude during a complex X-ray burst from soft gamma ray repeater J1550-5418 on 22 January 2009 starting at 05:17:43.6 UT and observed at ROI (black) and EACF (red) stations. The green lines show the time evolution of the X-ray count rate detected in ACS/SPI. The blue vertical line on the left represents the corresponding count rate of  $2 \times 10^5$  counts.s<sup>-1</sup>. NPM = Lualualei, Hawaii; EACF = Estação Antarctica Commandante Ferraz; ROI = Radio Observatorio do Itapetinga.

## 2. VLF Observation During SGR X-Ray Bursts

VLF data from two propagation paths (Figure 1) consisting of a single transmitter NPM and two receivers, namely, ROI and EACF, are used here for investigation. The total lengths of the propagation paths are 13,071 and 12,660 km, respectively. VLF observations are made with a time resolution of 20 ms. Among the total time window of observation on 22 January 2009, we are interested here in a small part of  $\sim 70$  s, during which both propagation paths were under nighttime condition. The temporal interval includes the VLF signal modification due to a so called complex X-ray bursts with multiple consecutive peaks starting at 05:17:43.6 UT. In Figure 1, the region under (south) the thick black line, showing the area of the Earth under illumination of the X-ray bursts on this occasion, clearly indicates that among the two propagation paths, the portion of total path illuminated by the bursts is much larger for NPM-EACF one than that of NPM-ROI. This explains why the deviation of VLF amplitude from undisturbed condition is much greater for NPM-EACF path than the other.

The mean undisturbed VLF amplitude  $A_0$  is a function of path length, transmission, and receiver properties and various propagation path characteristics. To nullify those effects and to demonstrate the comparative behavior of the change in VLF signal amplitude ( $\Delta A$ , primarily denoted by the deviation of amplitude from the corresponding undisturbed value  $A_0$ ), we use and show the relative amplitude change  $\frac{\Delta A}{A_0}$  as a function of time in Figure 2. In the figure, we also include the time evolution of X-ray count rate measured by the Anti-Coincidence Shield of the SPI (ACS/SPI) spectrometer on-board the INTEGRAL satellite (Mereghetti et al., 2009).

## 3. Probable Influence of Extraterrestrial X-Rays on VLF Propagation

The waveguide mode theory (Budden, 1961; Galejs, 1972; Wait, 1962), which conveniently describes long distance ( $>1,000$  km) propagation of VLF radio waves, assumes the horizontally stratified layers of the ionosphere and the surface of the Earth as the upper and lower boundary of a waveguide. The electromagnetic field at any point in this waveguide is decomposed into a series of independent field structures, called *modes*, propagating with different velocities. The vertical electric field strength between the ground and the ionosphere can be written as a sum of those waveguide modes (Lyn, 2010). The ionosphere is generally assumed to be inhomogeneous and anisotropic, and the ground is of finite conductivity, while the ionospheric and ground parameters should be changing with propagation path. With the increase in distances along propagation path, higher-order modes attenuate out, and the mode structure simplifies.

The refractive index for VLF radio waves in the ionosphere, which is a complex quantity consisting of a refractive and an absorptive term, determines the effective reflection height of the radio waves propagating in the waveguide. The effective reflection height is a function of the local properties of the medium, mainly, the plasma frequency ( $\omega_p$ ; which varies with altitude,  $h$ , as square root of electron number density  $N_e(h)$ ) and electron-neutral collision frequency ( $\nu_e$ ). It also has dependence on wave properties, such as frequency ( $\omega$ ), incidence angle ( $\psi$ ) of the wave in the ionospheric layer during reflection and propagation direction with

respect to the Earth's magnetic field, and so forth (Mitra, 1951). Efficient and advanced computer-based models, like International Reference Ionosphere (IRI) model (Rawer et al., 1978), provide satisfactory description of the electron and ion densities in undisturbed ionosphere. Empirical model such as Wait's formula (Wait & Spies, 1964), which approximates electron density profile of D region with a simple exponential expression, is also useful in analysis of VLF radio wave propagation. At any altitude, the ion-neutral collision rate is negligible compared to other collision rates, namely, the electron-ion and the electron-neutral ones. At heights above  $\sim 120$  km, the electron-ion collisions dominate (Schmitter, 2011); however, they are not relevant for VLF wave propagation since these waves do not reach these altitudes. It is the collision frequencies ( $\nu_e$ ) between electrons and neutrals particles, which plays the dominant role in VLF propagation. Among various speculated altitude dependent collision frequency profiles, the one prescribed by Kelley (2009) is the most refined and widely accepted. This is given by

$$\nu_e = 5.4 \times 10^{-10} n_n T_e^{\frac{1}{2}}, \quad (1)$$

where  $n_n$  is the neutral concentration, and  $T_e$  is the electron temperature. Though the collision frequency profile is originally described for daytime, we proceed in our simulation assuming that the profile holds also for the night time situation, so that any variation from daytime to nighttime is implied by the changes in electron temperatures and neutral concentrations only.

The interaction of oscillating electromagnetic field of the radio wave with the ions (free electron) and the presence of ion (electron)-neutral collisions cause absorption and reemission of the oscillating field at reflection height. Absorption of radio waves in the ionosphere also occurs during the passage of the wave through the ionizing layers of the atmosphere below the reflection height. The collisions between electrons, ions, and neutral molecules of the ionosphere transfer the propagating wave energy to the thermal energy and thus reduce the wave intensity.

During extraterrestrial transient events, like solar flares, GRBs, and SGR bursts, the enhanced extreme UV and/or X-ray radiation levels at the Earth's atmosphere cause sudden increase in the ionization rate and hence in electron and ion densities in the lower ionospheric heights and those below it. This types of changes are broadly termed as SIDs (Mitra, 1974). Typically, a SID is characterized by sudden rise of electron density due to ionization and gradual fall (recovery) due to various recombinations, attachment, and detachment processes between the electron, ions, and neutrals in that part of the atmosphere. Depending on the rate of ionization and the values of the recombination coefficients (most of which depend on the neutral density values), the electron density enhancement rate varies over altitudes. The result is the sudden change in the amount of absorption of VLF wave energy. The modified degree of absorption manifests in VLF signal modulation causing sudden increase or decrease from the ambient level (depending on the mode interference pattern) followed by gradual recovery to ambient signal values.

The interaction of radiation from nonsolar/extragalactic transients in Earth's atmosphere differs in certain aspects compared to solar transient events, such as

1. Due to the distance of cosmological order, unlike solar transients, for which both photons and charged particles reach the Earth's atmosphere, the radiation from such events essentially consist of energetic photons only.
2. Usually the spectra responsible for atmospheric ionization for such events are harder with higher energy photons, particularly hard X-rays and soft  $\gamma$ -rays. For solar flares, the part of the spectrum that effectively modifies the plasma property of ionosphere is soft X-ray (up to  $\sim 10$ – $12$  keV), which produces most of the ionization at heights above  $\sim 60$  km. Whereas for events like GRBs, SGRs, due to higher energy photon abundance, ionization occurs (by the photons in the energy range from  $\sim 10$  to  $\sim 200$  keV) at much lower altitudes (as low as  $\sim 20$  km above ground; Inan et al., 2007).
3. These events are generally much sharper in time evolution. Unlike solar eruptive events, such as solar flares, which can sustain for few minutes (small B and C class flares) up to few hours (large M and X class flares) and even for few days (solar proton events following CMEs), they last generally for few millisecond up to few seconds. So the disturbances they produce in the atmosphere is usually of much shorter time span, compared to the solar counterparts.

Also, usually it is to be expected, that, disturbances, produced by such nonsolar transient events, should be detectable at night time mostly. Though for very bright events, daytime signatures have also been observed, such as that described by Inan et al. (2007).

During the propagation of VLF with certain frequency  $\omega$ , the quantity  $\omega_r = \frac{\omega_p^2}{\nu}$  related to the ionosphere, also called the conductivity parameter (Wait & Spies, 1964), plays the most significant role. The electron density distribution with height changes continuously during and immediately after such ionizing events. Combined with the values of the collision frequency, the electron density distribution determines the conductivity parameter profile and hence govern the approximate reflection height and the amount of absorption. The electron density evolution on the other hand is regulated by two factors. First of which is evidently the ionization source parameters, like energy deposition rate and hence spectrum and time profile of the radiation from the source. Second, the ion chemistry, particularly the recombination coefficients, attachment, and detachment coefficients between electrons, ions and neutrals, play important role during the enhancement in ionization and particularly at the recovery time, when the source of enhanced ionization is absent. The collision frequencies between electron, ions and neutrals, which are generally functions of the neutral concentration and electron-ion temperature, on the other hand, may vary during such events. Though, during those ionizing radiation sources and even for events like intense solar flares, there may be huge level of ionization; it is usually insignificant enough compared to the neutral concentrations. So modulation in the collision frequencies by imposing any modification in the neutral density and electron-ion temperature during these events is negligible.

#### 4. The Model

For the details of the three step computational model, we would like to refer Palit et al. (2013) to the readers. Here we will outline only the basics of the processes used, emphasizing largely on the modifications done considering the differences of SGR transient sources compared to solar flares, regarding their influence on Earth's atmosphere as described in section 1.

##### 4.1. Atmospheric Ionization by X-Ray and $\gamma$ -Ray

The first step of the model is the calculation of the rate of ionization during the multiple SGR X-ray bursts at all relevant heights of the atmosphere. For this, a robust and well-established Monte Carlo detector simulation program GEANT4 (Agostinelli et al., 2003) is employed. We simulate the layered atmosphere of the Earth with efficient geometry model, included in the framework. The necessary atmospheric parameters, like neutral densities, temperature and pressures, are adopted from NASA-MSIS-E-90 atmospheric model (Hedin, 1991) for the part of the globe consisting the propagation paths investigated. All the necessary physics required for the study of photoionization, scattering, secondary electron ionization, and so forth are incorporated with well-developed electromagnetic physics module of GEANT4, where we set the lowest cutoff energy value of  $\sim 10$  eV to track down to the last of the ionization steps. Photons are employed as primary particles with primary generation class, for which a uniform spectrum with 1,000 (enough number for statistical significance and yet not very computationally intensive) photons in each of the energy divisions (kiloelectron volt (keV) bins) are used. Photons with energies from 1 to 200 keV are considered, while each of the primary particles in those bins is provided a random value in the keV range of the corresponding bin. Here, as we are interested only in finding altitude variation of ionization rates, which also depends on the angle of photon incidence, the problem is two-dimensional. To obtain the final information on the ionization rates at any given time during the period of consecutive bursts, we went through the following normalization procedure. First, we normalize each of the ionization-height profile corresponding to certain photon incidence angle, obtained from Monte Carlo simulation, with a model spectrum pertaining to that time. They are further adjusted over time with the normalized light curve and angle of incidence. We obtained the spectrum of the SGR bursts, required for our calculation, in the following manner.

The only instrument with a continuous SGR J1550-5418 coverage during the entire day of 22 January 2009 was the SPI/ACS instrument on board INTEGRAL satellite (Mereghetti et al., 2009). However, this instrument has a higher energy threshold ( $>80$  keV) and provides no energy resolution. During the whole day, about 200 bursts from the SGR were detected with the instrument. Among them, 84 were also detected by the INTEGRAL/IBIS/ISGRI instrument, and for which spectral information ( $>20$  keV) was available (Savchenko et al., 2010). Among all the bursts detected, 55 bursts occurred in the VLF observation window (04:15–08:20 UT), as described in Raulin et al. (2014).

FERMI Gamma-ray Burst Monitor (GBM) detected the SGR bursts on that day, though within a limited time period (van der Horst et al., 2012). The total time that GBM could not detect bursts from SGR J1550-5418 was  $\sim 11$  hr. This is partially due to the passage of the satellite through South Atlantic Anomaly (SAA) and also

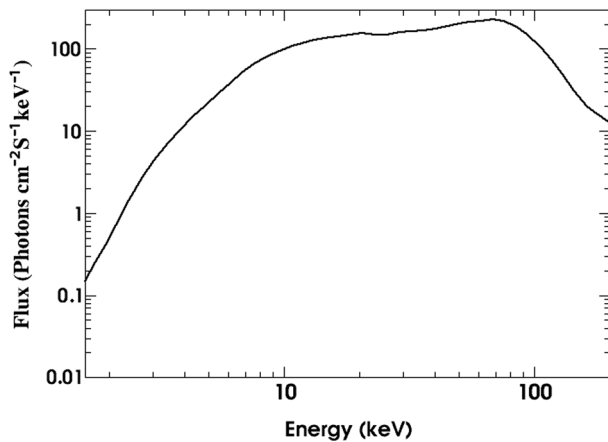


**Figure 3.** The base spectrum used in our calculation (adopted from Lin et al., 2012).

due to the occultation of SGR J1550-5418 by the Earth. van der Horst et al. (2012) made detail temporal and time-integrated spectral analysis of 286 SGR J1550-5418 bursts detected with GBM on that day. For those bursts, which caused saturation of the GBM detectors due to high count rates, analysis were done on the unsaturated parts of them only. One such spectral analysis for the unsaturated part of the burst occurring at 06:59:34 UT on 22 January 2009 is presented pictorially in the paper. Different physical model is employed for the fitting of spectrum, among which optically thin thermal bremsstrahlung spectrum best describes the data.

Lin et al. (2012) found 66 SGR J1550-5418 events from the same source, those are simultaneously observed with GBM (with energy band, 8–200 keV) and Swift/X-ray Telescope (energy band, 0.5–10 keV). They used 40 of such bursts, those occurred on 22 January of 2009, for broadband spectral analysis. The paper represents pictorially the broadband spectral modeling results of a single burst (at 2:34:28.194 UT on 22 January 2009), jointly fitted with the Comptonized model and the sum of two blackbody functions (BB + BB) models of the data from X-ray Telescope and GBM. The spectrum presented in Lin et al. (2012) is fitted in energies down to  $\sim 1$  KeV.

Mereghetti et al. (2009) computed the full ACS/SPI instrumental response (effective area as a function of energy) for observation of SGR J1550-5418 between 02:46 and 08:18 UT on 22 January 2009. Assuming an optically thin thermal bremsstrahlung spectrum convolved with ACS/SPI response and normalizing by comparing the integrated rate over energy of the test spectrum and observed one for each burst, they found an X-ray fluence of some of the bursts. In the same manner, Raulin et al. (2014) determined the fluence  $F_{25}$  (in 25 keV to 2 MeV energy range) of all the 55 bursts observed in the VLF observation window, with the help of X-ray observation data obtained with ACS/SPI (<http://www.isdc.unige.ch/integral/science/grb#ACS>) and put in tabular form in the article.

In this paper we adopted the same procedure as followed by Mereghetti et al. (2009) and Raulin et al. (2014) to calculate the fluence ( $F_{25}^0$ ) corresponding to the burst at 2:34:28.194 UT on 22 January 2009, for which Lin et al. (2012) presented the fitted spectrum. We also normalize the whole integral light curve in the VLF observation range to get the variation of fluence ( $F_{25}^t$ ) over time. The fitted spectrum as acquired from Lin et al. (2012) and presented here in Figure 3 is used as the base spectrum to calculate the electron density from the ionization-height profile in the Monte Carlo simulation. The normalized light curve during the whole VLF observation span is obtained by the ratio  $F_{25}^t/F_{25}^0$ .

For redundancy, we also carried out the same procedure for the burst at 06:59:34 UT, for which the spectrum is presented in van der Horst et al. (2012). Now, the fluence is calculated for the nonsaturated parts of the burst at 06:59:34 UT only. We adopted the spectrum of the nonsaturated part of the burst at 06:59:34 UT from van der Horst et al. (2012) and extrapolate it down to 1 keV with the help of a computer program, which follows the pattern and almost exactly reproduces the spectrum down to 1 keV, when applied to the spectrum presented at Lin et al. (2012), with lower cutoff set at 8 keV. Here we also want to mention that the part of the spectrum below  $\sim 10$  keV is the least influential in determining the ionosphere electron (ion) density and hence VLF signal modulation for sources like SGR bursts. This is because, for such sources, unlike solar flares, the spectrum is highly abundant in higher energies (up to  $\sim 100$  keV), and maximum ionization occurs at height well below  $\sim 60$  km. The part of the spectrum (below  $\sim 10$  keV), which should mainly contribute in ionization at  $\sim 70$ – $100$  km, is too less abundant in photons to produce any significant enhancement in electron (ion) densities to effect the VLF propagation. It implies that the accuracy of extrapolation of GBM spectrum down to 1 keV is of the least importance in this scenario. Use of either of the spectra in our model is found to generate identical outcome.

#### 4.2. Ion-Chemical Evolution

To estimate the time evolution of electron and ion densities in the lower ionosphere and the atmosphere below it due to various attachment, detachment and recombination processes, we use a five-constituent ion-chemistry model. This is an extension of the model employed in Palit et al. (2013), originally invoked by

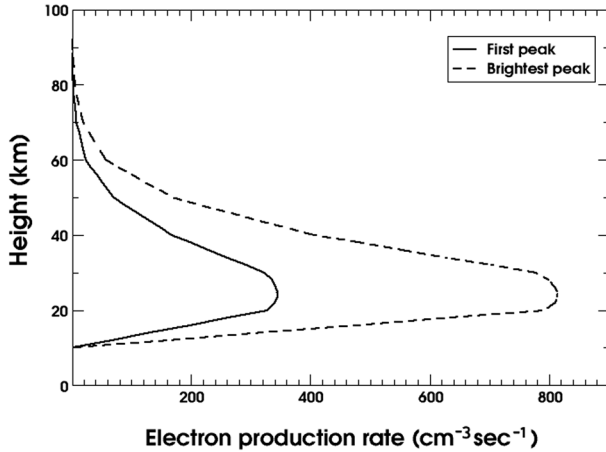


**Figure 4.** Calculated rates of ionization as function of height at the first peak (solid line) and the brightest peak (dashed line) of the complex burst presented in Figure 2.

Glukhov et al. (1992), where time evolution of lower ionospheric ion chemistry is determined by solving four coupled ordinary differential equations governing electron and ion production and loss rates for four broadly categorized electron, ion species concentrations. These are the electrons (concentration,  $N_e$ ), negative ions ( $N^-$ , consisting of  $O_2^-$ ,  $CO_3^-$ ,  $NO_2^-$ ,  $NO_3^-$ , etc.), light positive ions ( $N^+$ , composing of mainly  $O_2^+$  and  $NO_2^+$ ) and positive ion clusters ( $N_x^+$ , usually of the form  $H^+(H_2O)_n$ ). At heights below  $\sim 50$  km, heavy negative ions ( $N_x^-$ ), generated by interaction of negative ions, such as  $NO_3^-$  and its hydrates  $NO_3(H_2O)_n$  with neutral species, play important role in ion chemistry (E. E. Ferguson, 1979) and hence should necessary be included in the model. Most significant influence of the heavy negative cluster ions in the ion chemistry is due to their very high electron affinity (3.91 eV for  $NO_3^-$  and higher for the hydrates; Reid, 1979), which makes electron detachment virtually impossible (Lehtinen & Inan, 2007).

The differential equations governing the time evolution of the electron and ion densities, consisting of the contribution of various production (+ve terms) and loss (–ve terms) of ion species at right hand sides are given by

$$\frac{dN_e}{dt} = I + \gamma_e N^- + \gamma_x N_x^- - \beta_e N_e - (\alpha_d N^+ + \alpha_d^c N_x^+) N_e, \quad (2)$$

$$\frac{dN^-}{dt} = \beta_e N_e - \gamma_e N^- - \alpha_i N^- (N^+ + N_x^+) - AN^-, \quad (3)$$

$$\frac{dN_x^-}{dt} = -\gamma_x N_x^- - \alpha_i N_x^- (N^+ + N_x^+) + AN^-, \quad (4)$$

$$\frac{dN^+}{dt} = I - \alpha_d N_e N^+ - \alpha_i (N^- + N_x^-) N^+ - BN^+, \quad (5)$$

$$\frac{dN_x^+}{dt} = -\alpha_d^c N_e N_x^+ - \alpha_i (N^- + N_x^-) N_x^+ + BN^+. \quad (6)$$

The charge neutrality of the plasma requires

$$N_e + N^- + N_x^- = N^+ + N_x^+. \quad (7)$$

Here the parameter  $\beta_e$  is the electron attachment rate (Rowe et al., 1974), with a value,

$$\beta_e = 10^{-31} N_{O_2} N_{N_2} + 1.4 \times 10^{29} \left(\frac{300}{T_e}\right) e^{(-\frac{600}{T_e})} N_{O_2}^2, \quad (8)$$

where,  $T_e$  is the electron temperature, and  $N_{O_2}$  and  $N_{N_2}$  are the number densities of molecular oxygen and nitrogen, respectively. In the calculation of the parameter  $\beta_e$ , the neutral atom concentrations at different altitudes are obtained from NASA-MSIS-E-90 model (Hedin, 1991). The speculated value of electron detachment rate  $\gamma_e$  (Lehtinen & Inan, 2007; Pasko & Inan, 1994) varies widely in the range from  $10^{-23} N s^{-1}$  to  $10^{-16} N s^{-1}$ , where,  $N$  is the total neutral density. Following Glukhov et al. (1992), the value of  $\gamma_e$  is taken to be  $3 \times 10^{-18} N s^{-1}$ . The value of the effective coefficient of dissociative recombination  $\alpha_d$  may vary from  $10^{-7}$  to  $3 \times 10^{-7} cm^3/s$  (Lehtinen & Inan, 2007; Rowe et al., 1974). Following previous studies, we have used  $3 \times 10^{-7} cm^3/s$  for  $\alpha_d$ . The value of effective recombination coefficient of electrons with positive cluster ions  $\alpha_d^c$  has a variation in the range  $\sim 10^{-6} - 10^{-5} cm^3/s$ , whereas the value of the effective coefficient ( $\alpha_i$ ) of ion-ion recombination processes for all types of positive ions with negative ions is taken to be  $10^{-7} cm^3/s$  (Mitra, 1968; Rowe et al., 1974). Here the value of  $10^{-5} cm^3/s$  is adopted for  $\alpha_d^c$  as suggested by Glukhov et al. (1992).  $B$  is the effective rate of conversion from the positive ions ( $N^+$ ) to the positive cluster ions ( $N_x^+$ ) and has a value  $10^{-30} N^2 s^{-1}$  (Mitra, 1968; Rowe et al., 1974), in agreement with Glukhov et al. (1992). The detachment rate ( $\gamma_x$ ) of electrons from heavy negative ions differs in daytime and nighttime, with probable daytime value of 0.002/s and night time value of 0 (Reid, 1979). According to Lehtinen and Inan (2007), the parameter  $A$ , denoting the rate of conversion from light negative ion to negative cluster ions has a value between  $3 \times 10^{-20} N s^{-1}$  and  $10^{-18} N s^{-1}$ . We use for  $A$  the value of  $10^{-19} N s^{-1}$ . From the discussion above, we see that there is ambiguity in the values of most of the parameters. This is attributed to the fact that, unlike other parts of the ionosphere and Earth's atmosphere, there is no convenient way of direct measurement of the characteristics of lower part of the ionosphere. So there is no way of getting estimate of such values other than indirect measurements through remote sensing,

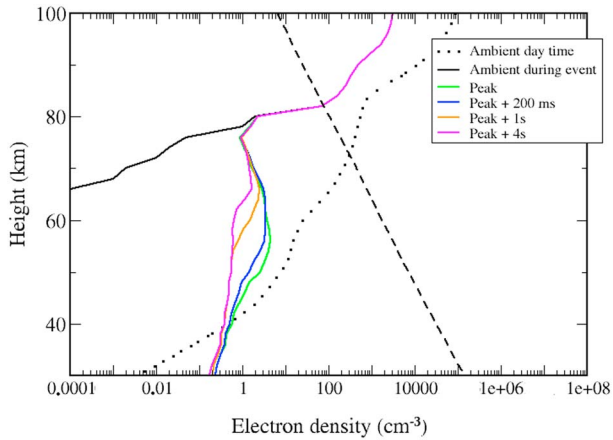


**Figure 5.** The figure shows the electron density distribution (colored curves) as function of height, calculated at EACF site and the approximate values of electron densities required for the VLF reflection at each heights for Kelley's (black-dashed line) collision frequency profile. Ambient electron density during event (black solid line), daytime ambient electron density (black-dotted line), those during the maximum (X-ray) of brightest peak, and at various times of the recovery phases are shown with different colors.

laboratory experiments, and numerical simulations. This also makes the efforts to properly interpret any remote observation of this part of the atmosphere, such as through VLF radio waves extremely challenging. Hence, the liberty of investigating with various values of those parameters might be taken during such model.

At night, the ionization rate per unit volume ( $I = I_0 + I_t$ ) should consist of two terms. One is from the cosmic ray contribution ( $I_0$ ), responsible for maintaining the ionospheric structure at night time in absence of solar ultraviolet radiation. The other term ( $I_t$ ) is due to the ionization by the X-ray and  $\gamma$ -ray from the SGR bursts. For the ionospheric heights for which the ambient electron and ion densities at night time are known, such as from IRI model (Rawer et al., 1978), we can easily find out the approximate rate of ionization ( $I_0$ ) from cosmic rays to maintain the night time electron density. This can be done by solving the rate equations simultaneously, provided the values of the rate coefficients are known. But for most of the heights (below  $\sim 70$  km) we are concerned with, IRI model does not give any electron and ion concentration values at night time. Even for those heights, for which the electron/ion densities may be known from IRI model at the start of the model calculation (in our case, most suitably at day-night terminator time),  $I_0$  can be calculated with some extra efforts. Here we adopt a more convenient method to calculate the ambient ionization due to cosmic ray suggested by Lehtinen and Inan (2007). We use an empirical cosmic ray source of ionization, roughly following the cosmic ray flux attenuation through atmosphere, given by

$$Q = Q_{\max} \left( \frac{N}{N_{\max}} \right) e^{\left( 1 - \frac{N}{N_{\max}} \right)}, \quad (9)$$

where,  $N$  is the neutral density,  $N_{\max}$  is that at the ionization production peak altitude  $h_{\max}$ , which is initially taken to be  $\sim 15$  km following Reid (1979).  $Q_{\max}$  is the electron production rate by cosmic ray at  $h_{\max}$ . Depending on the choice of the chemical rate coefficients, the values of  $Q_{\max}$  and  $h_{\max}$  are adjusted so that the rate equations give a steady electron density distribution over the required height range.

With the knowledge of  $I_0$  and using the ionization rate per unit volume ( $I_t$ ), obtained from GEANT4 simulation and the rate coefficients, we solve the ordinary differential equations (equations (2)–(6)) by fourth-order explicit Runge-Kutta method to find the residual electron density at various altitudes during the course of the flare. The time increment of the calculation is adjusted over heights, as the values of rate coefficients, like  $\beta_e$  and  $\gamma_{er}$ , and hence rate of change of concentrations vary widely (up to a factor of  $\sim 8$ ) in the considered height range. In the whole process, thorough care of the charge neutrality condition is taken into account.

### 4.3. Waveguide Mode Calculation with LWPC

Current version of LWPC (J. A. Ferguson, 1998), which is a very versatile and well-known code for calculation of VLF propagation characteristics over long propagation paths based on waveguide mode theory, allows to include arbitrary ionospheric variations as an input assumption. This includes the electron density and the collision frequency values as a function of height. The electron density as function of height calculated from the ion chemistry model is set as input in the LWPC code. In LWPC, each propagation path is characterized by the transmitter characteristic parameters, like position in latitude and longitude, transmission frequency, distance to receiver, and corresponding bearing angle. For greater accuracy, we divide each propagation paths as stated above, into four horizontal segments and input columnar electron density values calculated at the midpoints of each region. We have found that division in greater number of segments does not have any demonstrable effect or improvement in the results. First, we perform our LWPC run with the ambient electron densities, estimated over the propagation paths, which remain almost constant over the small time period of calculation ( $\sim 70$  s). Then we perform our calculation with the disturbed electron density profile at each interval of 0.2 s. For those times when the changes are very rapid, such as at the peak of each burst, we make more frequent LWPC runs (0.05 s). We found that the time interval chosen in such a way is sufficient to reproduce the features of VLF modulation reasonably. We use Kelley's collision frequency profile (equations (1)) in LWPC calculations. In the next section, we show our model results.

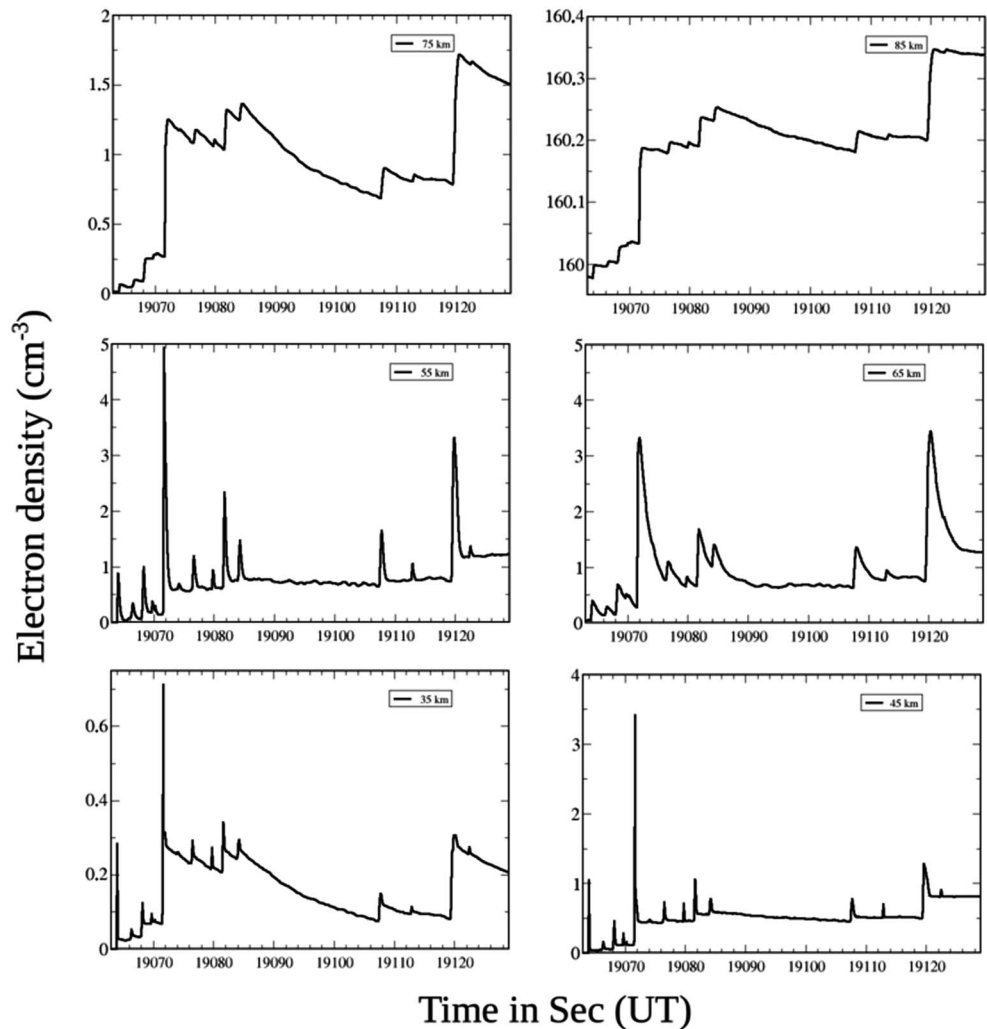


**Figure 6.** Electron density evolution during the complex burst at various heights as calculated from ion-chemistry model.

### 5. Results

In Figure 4, we show the rate of ionization as function of height calculated from GEANT4 simulation above the location of receiver EACF for two different times of the complex burst presented in Figure 2. The solid line represents the ionization rate during the first of the peak at 05:17:43.6 UT, and the dashed curve is that for the brightest peak at 05:17:51.6 UT. Our simulation shows that ionization extends to height as low as  $\sim 10$  km, with the maximum occurring at  $\sim 24$  km. It is the hard X-ray and the softer  $\gamma$ -ray parts of the photon energy range ( $\sim 20$ – $200$  keV), which affects the ionization most due to the SGR bursts. The heights for the maximum of ionization and electron density are not same as can clearly be seen in Figure 5. The solid black and green curves in Figure 5 represent, respectively, the calculated ambient electron density and that at the time of maximum ionization during the brightest peak at the EACF location. Though the ionization rate is maximum at about  $\sim 24$  km, the high recombination rates at those heights prevent the large accumulation of free electrons during the very short duration of the SGR X-ray burst. Steeply decreasing values of recombination rates with increasing height cause the occurrence of maximum electron density at height ( $\sim 55$  km) much above that of the maximum ionization. Due to various recombination processes the enhanced electron density gradually diminishes from its peak value. The other colored curves represent the electron density during the recovery phase, after 200 ms (blue), 1 s (orange), and 4 s (pink) of the peak of ionization. From the expression of effective reflection height (Mitra, 1951), we can calculate the approximate (putting the value of  $\sin^2 \psi$  to 1) values of electron densities required for VLF reflection to occur at different heights for the given collision frequency profile. The point at which one such plot intersects a given electron density-height profile should

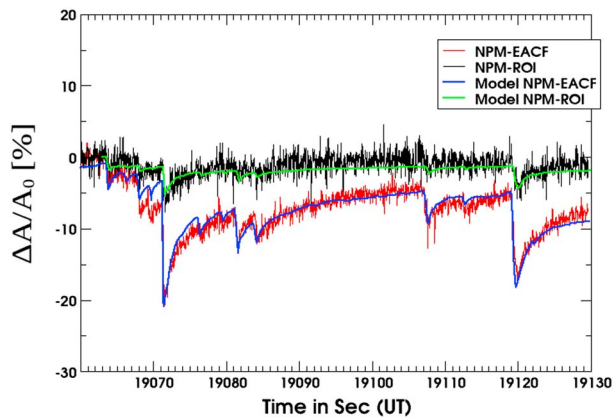


**Figure 7.** Normalized very low frequency amplitude modulations during the complex burst. The black and red lines are the observed ROI and EACF profiles, respectively. The green curve is the modeled very low frequency amplitude evolution for the ROI station, and the blue curve is that for EACF station. NPM = Luualalei, Hawaii; EACF = Estação Antarctica Commandante Ferraz; ROI = Radio Observatorio do Itapetinga.

provide us the approximate reflection height at that condition. In Figure 5, the black-dashed line represents the calculated electron densities required at various heights for the effective reflection of VLF waves for collision frequencies given by Kelley (equations (1)). For the calculation of Kelley's collision frequency profile, the neutral density values are obtained from NASA-MSIS-E-90 atmospheric model (Hedin, 1991). We can see from the figure that the approximate reflection heights are greater than 80 km for both ambient condition and during the event, that is well above the heights ( $\sim 30\text{--}70$  km) where electron and related ion densities are enhanced after ionization by X-rays and  $\gamma$ -rays from the SGR-bursts. There is virtually no change in the effective reflection height during the event from that during ambient condition at the time. This clearly suggests that for night time, any modification in VLF signal during the SGR X-ray bursts is not imposed by a change in effective reflection height but is solely dominated by the absorption at heights well below it. If similar X-ray bursts had occurred in daytime, then the ambient reflection height ( $\sim 70$  km, as can be seen from the position of the point of intersection of the black-dashed line and the daytime ambient electron density profile) would have been slightly modified by the electron density enhancement caused by the SGR bursts.

In Figure 6, we show the calculated electron density evolution as function of time during the entire complex burst for different heights. During any of the bursts, the variation in the slope of decay of the electron densities from the corresponding peak values, as seen in the Figure 6, can be attributed to the variation of the rates of chemical processes over heights. Though the implications are not quite clear, we note that the observed VLF amplitude modulation seems to closely follow the time evolution of simulated electron density at  $\sim 66$  km. In Figure 7, we show the modeled VLF amplitude variation over the considered time window for both the NPM-ROI (green) and NPM-EACF (blue) propagation paths using Kelley's collision frequency and compare them with the observed VLF profiles (black for NPM-ROI and red for NPM-EACF paths). It definitely appears that apart from slight mismatch at the recovery phases following the initial enhancements during most of the peaks, the modeled profiles follow the observed ones quite closely. The slight discrepancies can be attributed to the lack of exact knowledge of the values of the adopted chemical rate parameters and, hence, blunt adoption of some parameters like  $\gamma_e$ ,  $\beta_e$ ,  $\alpha_d$ , and  $\alpha_d^c$  in their proposed ranges. In future, we aim to improve our ion-chemistry model by treating all the ion species individually instead of grouping them and replacing single-averaged rate coefficient for each group with the cross section of each individual chemical reactions involved in the part of the atmosphere. Some existing advanced models such as Sodankylä Ion-Neutral Chemistry model (Turunen et al., 1996) or the Whole Atmosphere Community Climate Model (Garcia et al., 2007) may also be used for improved replication of the observation.

## 6. Concluding Remarks

In this paper, we exercise the reconstruction of the modulation of VLF amplitude observed during a complex X-ray burst from a SGR with a three-step computation model comprising of (i) ionization rate estimation with GEANT4-based Monte Carlo simulation, (ii) ionospheric chemistry model based on modified GPI scheme, and (iii) simulation of subionospheric VLF signal propagation with LWPC code. Instead of the usual and most popular approach of modeling of such events by varying Wait's parameters, we have used a more realistic method starting from actual observed X-ray and  $\gamma$ -ray flux and modeled spectrum from Space instruments. When possible, this is the most suitable approach of analyzing such observed events in terms of accuracy and closeness to real physical and chemical processes responsible for such modulations. Very few and justifiable assumptions are made during the calculations. In addition to the fulfillment of our primary target, that is, the reconstruction of VLF signal modulation through extended computer simulation, we have also acquired some understanding on the modifications of the atmospheric properties under such ionizing disturbance, like the rate of production of ionization and time evolution of electron and ion density (though not shown here explicitly) values at different heights of the middle atmosphere and lower ionosphere.

Despite the fact that the knowledge of the chemical processes related to the ions and electrons at lower-ionospheric heights and the atmospheric layers just below it, where the effect of such cosmic ionizing

sources is felt most, is not quite exact, we have been able to reproduce the observed signal amplitude quite satisfactorily. More accurate reconstruction of the observed signal will require more precise and improved knowledge of the ion and neutral chemistry parameters at ionospheric and middle atmospheric heights.

Each of the stand-alone peaks during such X-ray bursts from SGR, appearing in the model, can be considered as point source in terms of temporal variation in ionization. Then, these simple bursts provide a promising way to determine the response of the atmosphere to point like ionizing agents or spikes. This has the potential to contribute valuable information on the dynamics of D region and layers of atmosphere below it in terms of the chemistry of the region. In a near future, in addition to further improvement of our model, we will also concentrate on this very interesting aspect.

#### Acknowledgments

Sourav Palit acknowledges a grant from FAPESP (file -2016/02550-6) for financial support. J. P. R. would like to thank the National Council for Research and Development (CNPq; proc. 312066/2016-3) for the received support. E. C. also thanks CNPq for individual research support (processes nos. 406690/2013-8 and 303299/2016-9). The observed VLF data are available at Centro de Radio Astronomia e Astrofísica Mackenzie, CRAAM, Universidade Presbiteriana Mackenzie.

#### References

- Agostinelli, S., Allison, J., Amako, K., Apostolakis, J., Araujo, H., Arce, P., et al. (2003). GEANT4 simulation toolkit. *Nuclear Instruments and Methods in Physics A*, *506*, 250–303.
- Budden, K. G. (1961). *The Wave-Guide Mode Theory of Wave Propagation: A Mathematical Treatment of the Propagation of Radio Waves at Great Distance Over Land and Through Water*. Prentice-Hal, London, Englewood Cliffs, NJ: Logos Press-Elek Books and Ltd.
- Cohen, M. B., Inan, U. S., & Paschal, E. P. (2009). Sensitive broadband ELF/VLF radio reception with the AWESOME instrument. *IEEE Transactions on Geoscience and Remote Sensing*, *48*, 3–17. <https://doi.org/10.1109/TGRS.2009.2028334>
- Ferguson, E. E. (1979). Ion chemistry of the middle atmosphere. In *NASA Conf. Publ., CP-2090* (pp. 71–88).
- Ferguson, J. A. (1998). Computer programs for assessment of long-wavelength radio communications, version 2.0 (Technical document 3030). San Diego, CA: Space and Naval Warfare Systems Center.
- Fishman, G. J., & Inan, U. S. (1988). Observation of an ionospheric disturbance caused by a gamma-ray burst. *Nature*, *331*, 418–420.
- Galejs, J. (1972). *Terrestrial Propagation of Long Electromagnetic Waves*. New York: Pergamon Press.
- Garcia, R. R., Marsh, D. R., Kinnison, D. E., Boville, B. A., & Sassi, F. (2007). Simulation of secular trends in the middle atmosphere, 1950–2003. *Journal of Geophysical Research*, *112*, D09301. <https://doi.org/10.1029/2006JD007485>
- Glukhov, V. S., Pasko, V. P., & Inan, U. S. (1992). Relaxation of transient lower ionospheric disturbances caused by lightning-whistler induced electron precipitation bursts. *Journal of Geophysical Research*, *97*, 16,971–16,979.
- Grubor, D. P., Šulić, D. M., & Žigman, V. (2008). Classification of X-ray solar flares regarding their effects on the lower ionosphere electron density profile. *Annals of Geophysics*, *26*, 1731–1740.
- Hargreaves, J. K. (1992). *The Solar-Terrestrial Environment*. New York: Cambridge University Press.
- Hedin, A. E. (1991). Extension of the MSIS Thermosphere Model into the middle and lower atmosphere. *Geophysical Research Letters*, *96*, 1159–1172.
- Hurley, K., Clint, T., Mazets, E., Barthelmy, S., Butterworth, P., Marshall, F., et al. (1999). A giant periodic flare from the soft  $\gamma$ -ray repeater SGR1900+14. *Nature*, *397*(6714), 41–43.
- Inan, U. S., Lehtinen, N. G., Moore, R. C., Hurley, K., Boggs, S., Smith, D. M., & Fishman, G. J. (2007). Massive disturbance of the daytime lower ionosphere by the giant  $\gamma$ -ray flare from magnetar SGR 1806-20. *Journal of Geophysical Research*, *34*, L08103. <https://doi.org/10.1029/2006GL029145>
- Kelley, M. C. (2009). *The Earth's Ionosphere, Plasma Physics and Electrodynamics* (Chap. 2.2, 2nd ed.). Amsterdam: Academic Press.
- Kolarski, A., & Grubor, D. (2014). Sensing the Earth's low ionosphere during solar flares using VLF signals and goes solar X-ray data. *Advances in Space Research*, *53*(11), 1595–1602.
- Lehtinen, N. G., & Inan, U. S. (2007). Possible persistent ionization caused by giant blue jets. *Geophysical Research Letters*, *34*, L08804. <https://doi.org/10.1029/2006GL029051>
- Lin, L., Göğüş, E., Baring, M. G., Granot, J., Kouveliotou, C., Kaneko, Y., et al. (2012). Broadband spectral investigations of SGR J1550-5418 bursts. *The Astrophysical Journal*, *756*(54), 12. <https://doi.org/10.1088/0004-637X/756/1/54>
- Liu, J. U., Chiu, C. S., & Lin, C. H. (1996). The solar flare radiation responsible for sudden frequency deviation and geomagnetic fluctuation. *Journal of Geophysical Research*, *101*, 10,855–10,862.
- Lyn, J. W. (2010). VLF waveguide propagation: The basics. In *AIP Conference Proceedings 1286*, 3 (2010) (pp. 3–41). <https://doi.org/10.1063/1.3512893>
- Mariska, J. T., & Oran, E. S. (1981). The E and F region ionospheric response to solar flares: 1. Effects of approximations of solar flare EUV fluxes. *Journal of Geophysical Research*, *86*, 5868–5872.
- Mathews, J. D., Breakall, J. K., & Ganguly, S. (1982). The measurement of diurnal variations of electron concentration in the 60-100 km ionosphere at Arecibo. *Journal of Atmospheric and Terrestrial Physics*, *44*, 441–448.
- McRae, W. M., & Thomson, N. R. (2004). Solar flare induced ionospheric D-region enhancements from VLF phase and amplitude observations. *Journal of Atmospheric and Solar-Terrestrial Physics*, *66*, 77–87.
- Mendillo, M., Klobuchar, J. A., Fritz, R. B., da Rosa, A. V., Kersley, L., Yeh, K. C., et al. (1974). Behavior of the ionospheric F region during the great solar flare of August 7, 1972. *Journal of Geophysical Research*, *79*, 665–672.
- Mereghetti, S., Goöz, D., Weidenspointner, G., von Kienlen, A., Esposito, P., Tiengo, A., et al. (2009). Strong bursts from the anomalous X-ray pulsar IE 1547.0-5408 observed with the INTEGRAL/SPI anti-coincidence shield. *The Astrophysical Journal*, *606*, L74–L78.
- Mitra, A. P. (1951). The D layer of the ionosphere. *Journal of Geophysical Research*, *56*(3), 373–402.
- Mitra, A. P. (1968). A review of D-region processes in non-polar latitudes. *Journal of Atmospheric and Solar-Terrestrial Physics*, *30*, 1065–1114.
- Mitra, A. P. (1974). Ionospheric effects of solar flares. In *Astrophysics and Space Science Library, Book Series*. Dordrecht 46: Springer.
- Mondal, K., Chakrabarti, S. K., & Sasmal, S. (2012). Detection of ionospheric perturbation due to a soft gamma ray repeater SGR J15505418 by very low frequency radio waves. *Astrophysics and Space Science*, *341*, 259–264.
- Nicolet, M., & Aikin, A. C. (1960). The formation of the D region of the ionosphere. *Journal of Geophysical Research*, *65*, 1469–1483.
- Nina, A., Simić, S., Srećković, V. A., & Popović, L. Č. (2015). Detection of short-term response of the low ionosphere on gamma ray bursts. *Geophysical Research Letters*, *42*, 8250–8261. <https://doi.org/10.1002/2015GL065726>
- Nina, A., & Čadež, V. M. (2014). Electron production by solar Ly- $\alpha$  line radiation in the ionospheric D-region. *Astrophysics and Space Science*, *54*, 1276–1284.

- Palit, S., Basak, T., Mondal, S. K., Pal, S., & Chakrabarti, S. K. (2013). Modeling of very low frequency (VLF) radio wave signal profile due to solar flares using the GEANT4 Monte Carlo simulation coupled with ionospheric chemistry. *Atmospheric Chemistry and Physics*, *13*, 9159–9168. <https://doi.org/10.5194/acp-13-9159-2013>
- Palit, S., Basak, T., Pal, S., & Chakrabarti, S. K. (2015). Theoretical study of lower ionospheric response to solar flares: Sluggishness of D-region and peak time delay. *Astrophysics and Space Science*, *356*, 19–28.
- Palit, S., Ray, S., & Chakrabarti, S. K. (2016). Inverse problem in ionospheric science: Prediction of solar soft-X-ray spectrum from very low frequency radiosonde results. *Astrophysics and Space Science*, *361*, 151. <https://doi.org/10.1007/s10509-016-2724-1>
- Pasko, V. P., & Inan, U. S. (1994). Recovery signatures of lightning associated VLF perturbations as a measure of the lower ionosphere. *Journal of Geophysical Research*, *99*, 17,523–17,537.
- Qian, L., Burns, A. G., Solomon, S. C., & Chamberlin, P. C. (2012). Solar flare impacts on ionospheric electrodyamics. *Geophysical Research Letters*, *39*, L06101. <https://doi.org/10.1029/2012GL051102>
- Raulin, J. P., Trottet, G., deCastro, C. G., Correia, E., & Macotela, E. L. (2014). Nighttime sensitivity of ionospheric VLF measurements to X-ray bursts from a remote cosmic source. *Journal of Geophysical Research: Space Physics*, *119*, 4758–4766. <https://doi.org/10.1002/2013JA019670>
- Raulin, J. P., Trottet, G., Kretzschmar, M., Macotela, E. L., Alessandra, P., Bertoni, F. C., & Dammach, I. E. (2013). Response of the low ionosphere to X-ray and Lyman- $\alpha$  solar flare emissions. *Journal of Geophysical Research: Space Physics*, *118*, 570–575. <https://doi.org/10.1029/2012JA017916>
- Rawer, K., Bilitza, D., & Ramakrishnan, S. (1978). Goals and status of the international reference ionosphere. *Reviews of Geophysics*, *16*, 177–181.
- Reid, G. C. (1979). The middle atmosphere. In *NASA Conf. Publ., CP-2090* (pp. 27–42).
- Rowe, J. N., Mitra, A. P., Ferraro, A. J., & Lee, H. S. (1974). An experimental and theoretical study of the D-region II. A semi-empirical model for mid-latitude D-region. *Journal of Atmospheric and Solar-Terrestrial Physics*, *36*, 755–785.
- Savchenko, V., Neronov, A., Beckmann, V., Produit, N., & Walter, R. (2010). SGR-like flaring activity of the anomalous X-ray pulsar 1E 1547.0-5408. *Astronomy and Astrophysics*, *510*, A77. <https://doi.org/10.1051/0004-6361/200911988>
- Schmitter, E. D. (2011). Remote sensing planetary waves in the midlatitude mesosphere using low frequency transmitter signals. *Annals of Geophysics*, *29*, 1287–1293.
- Schmitter, E. D. (2013). Modeling solar flare induced lower ionosphere changes using VLF/LF transmitter amplitude and phase observations at a midlatitude site. *Annals of Geophysics*, *31*, 765–773.
- Tanaka, Y. T., Terasawa, T., Kawai, N., Yoshida, A., Yoshikawa, I., Saito, Y., et al. (2007). Comparative study of the initial spikes of soft gamma-ray repeater giant flares in 1998 and 2004 observed with Geotail: Do magnetospheric instabilities trigger large-scale fracturing of a magnetars crust? *The Astrophysical Journal*, *665*, L55–L58.
- Tanaka, Y. T., Terasawa, T., Yoshida, M., Horie, T., & Hayakawa, M. (2008). Ionospheric disturbances caused by SGR 1900+14 giant-gamma ray flare in 1998: Constraints on the energy spectrum of the flare. *Journal of Geophysical Research*, *113*, A07307. <https://doi.org/10.1029/2008JA013119>
- Thomson, N. R., & Clilverd, M. A. (2001). Solar flare induced ionospheric D-region enhancements from VLF amplitude observations. *Journal of Atmospheric and Solar-Terrestrial Physics*, *63*, 1729–1737.
- Thomson, N. R., Clilverd, M. A., & Rodger, C. J. (2005). Large solar flares and their ionospheric D region enhancements. *Journal of Geophysical Research*, *110*, A06306. <https://doi.org/10.1029/2005JA011008>
- Turunen, E., Matveinen, H., Tolvanen, J., & Ranta, H. (1996). D-region ion chemistry model. In *STEP Handbook of Ionospheric Models*. Boulder, CO: SCOSTEP Secretariat.
- Usoskin, I. G., Desorgher, L., Velinov, P., Storini, M., Flückiger, E. O., Bütikofer, R., & Kovaltsov, G. A. (2009). Ionization of the Earth's atmosphere by solar and galactic cosmic rays. *Acta Geophysica*, *57*, 88–101.
- van der Horst, A. J., Kouveliotou, C., Gorgone, N. M., Kaneko, Y., Baring, M. G., Guiriec, S., et al. (2012). SGR J1550-5418 bursts detected with the Fermi gamma-ray burst monitor during its most prolific activity. *The Astrophysical Journal*, *749*, 122.
- Velinov, P., Asenovski, S., Kudela, K., Lastovicka, J., Mateev, L., Mishev, A., & Tonev, P. (2013). Impact of cosmic rays and solar energetic particles on the Earth's ionosphere and atmosphere. *Journal of Space Weather and Space Climate*, *3*, A14. <https://doi.org/10.1051/swsc/2013036>
- Wait, J. R. (1962). Introduction to the theory of VLF propagation. In *Proceedings of the IRE 50* (pp. 1624–1647).
- Wait, J. R., & Spies, K. P. (1964). Characteristics of the Earth-ionosphere waveguide for VLF radio waves (NBS Tech. Note 300). Washington, DC: U.S. Department of Commerce, National Bureau of Standards.
- Watanabe, K. (1958). Ultraviolet absorption processes in the upper atmosphere. *Advances in Geophysics*, *5*, 153–221.
- Watanabe, K., Marmo, F. F., & Pressman, J. (1955). Formation of the lower ionosphere. *Journal of Geophysical Research*, *60*, 513–519.
- Žigman, V., Grubor, D., & Šulić, D. (2007). D-region electron density evaluated from VLF amplitude time delay during X-ray solar flares. *JASTP*, *69*(7), 775–792.